This paper has been accepted for publication in Robotica, 2020.

Robotica (2020) © Cambridge University Press 2020

doi:10.1017/xxxx

Using a Redundant User Interface in Teleoperated Surgical Systems for Task Performance Enhancement

Ali Torabi†*, Mohsen Khadem‡, Koroush Zareinia ℵ,

Garnette Roy Sutherland§, and Mahdi Tavakoli†

†*Department of Electrical and Computer Engineering, University of Alberta, Edmonton, AB, Canada*

‡ *School of Informatics, University of Edinburgh, Edinburgh, UK*

ℵ*Department of Mechanical and Industrial Engineering, Ryerson University, Toronto, ON, Canada*

§*Project neuroArm, Faculty of Medicine, University of Calgary, Calgary, AB, Canada*

(Accepted MONTH DAY, YEAR. First published online: MONTH DAY, YEAR)

SUMMARY

The enhanced dexterity and manipulability offered by master-slave teleoperated surgical systems have significantly improved the performance and safety of minimally invasive surgeries. However, effective manipulation of surgical robots is sometimes limited due to the mismatch between the slave and master robots' kinematics and workspace. The purpose of this paper is first to formulate a quantifiable measure of the combined master-slave system manipulability. Next, we develop a null-space controller for the redundant master robot that employs the proposed manipulability index to enhance the performance of teleoperation tasks by matching the kinematics of the redundant

* Corresponding author. E-mail: ali.torabi@ualberta.ca

master robot to the kinematics of the slave robot. The null-space controller modulates the redundant degrees of freedom of the master robot to reshape its manipulability ellipsoid towards the manipulability ellipsoid of the slave robot. The manipulability ellipsoid is the geometric interpretation of the kinematics of a robot. By reshaping the master robot's manipulability, we match the master and slave robots' kinematics. We demonstrate that by using a redundant master robot, we are able to enhance the master-slave system manipulability and more intuitively transfer the slave robot's dexterity to the user. Simulation and experimental studies are performed to validate the performance of the proposed control strategy. Results demonstrate that by employing the proposed manipulability index, we can enhance the user's control over the force/velocity of a surgical robot and minimize the user's control effort for a teleoperated task.

KEYWORDS: Teleoperation; Haptic Interfaces; Medical Robots and Systems; Redundant Manipulators; Null-space Control.

1. Introduction

Teleoperated robotic systems can significantly enhance a surgeon's accuracy and performance by utilizing advantages offered by a robotic system such as enhanced dexterity and manipulability. Master-slave teleoperation is a common and effective means of providing an intuitive user interface for controlling surgical robots. The slave robot, in the context of the surgery, is the actual surgical manipulator that performs the surgery, while the master is a device that allows the surgeon to control the slave while providing visual/force feedback to the user to improve the safety of the procedure. The enhanced dexterity offered by teleoperated surgical robots allows for precise, dexterous control of the slave robot [1]. The master robot, which is critical to the safety and success of any interaction, requires appropriate design and control [2]. Performance and design requirements of master robots are given in [3–5]. There are trade-offs between the desirable characteristics of the master robots which can be relaxed by using kinematically redundant robots. A redundant manipulator has more degrees of freedom (DoF) than

required to perform a task. Redundant robots are often employed to perform complicated tasks that require a high level of dexterity, such as obstacle avoidance or manipulability enhancement [6].

Several researchers have used redundant master or slave robots to enhance the dexterity of master-slave robotic systems [7–11]. It has been shown that in human-machine interaction, the redundant robot is important to the overall performance of the task [12]. The human arm and fingers have kinematic redundancy [13]. Studies have shown that human users employ kinematic redundancies in their arm along with compliant task space control to perform complex dexterous tasks [14]. Also, in a recent study on the performance of experienced surgeons, it was shown that they exploit their arm's redundancy to stabilize hand movements more than novice surgeons [15].

Das *et al.* [10] were among the first researchers that employed kinematic redundancy and a kinematic controller for the slave robot to avoid obstacle collision in a teleoperation scenario. Hwang *et al.* [8] developed a framework for evaluating the performance of a teleoperation system where only the slave system was a redundant robot manipulator. Despite the promising features of redundant master robots, only limited attention has been paid to their design and control. One of the first redundant master robots was introduced in [16]. They proposed an admittance controller to control the robot due to its relatively large dynamic properties, such as large apparent inertia. Nath *et al.* [9] studied the teleoperation of redundant manipulators when the master and slave robots have the same degrees of freedom. The well-known da Vinci Surgical System (Intuitive Surgical, Inc. CA, USA) also benefits from a redundant 7 DoF Master robot [17]. Application of dexterous redundant robots in teleoperation is limited as there is no quantifiable measure of dexterity for the teleoperated robotic system.

One of the well-established tools for motion and dexterity analysis of robot manipulators is the manipulability ellipsoid (ME) [18]. This geometric measure indicates the ability to perform motion and exert force along the different task directions in a given joint configuration [19]. Manipulability of robots was first introduced in [18] to describe

how a manipulator can move in arbitrary directions, and to quantify the ability to perform an action quickly and skilfully [20]. Manipulability analysis consists of describing the motion of the robot in the task as a function of a measure of the robot's effort in joint space (e.g., joint torque). Yoshikawa defined a quality measure based on the analysis of the ME. ME is a volume/surface in the Cartesian velocity space, which is mapped from the unit sphere in the joint velocity space by a Jacobian transformation [18].

Researchers have studied the application of the manipulability index in the design and control of surgical robots. Konietschke *et al.* [21] and Li *et al.* [22] used the manipulability index for optimal design of a dexterous surgical robot. From our group, Torabi *et al.* [23] used the manipulability as a criterion to modify the design of currently existing master-slave robotic systems to improve the performance of teleoperation surgery. They introduced the teleoperation manipulability ellipsoid as a measure of manipulability for teleoperated master-slave robotic systems. The teleoperation ME is defined as the volume of the intersection between the MEs for the individual arms, where the intersection of the two MEs is subject to the constraints imposed by the teleoperation system. In an experimental study, Maddahi *et al.* [24] demonstrated the relation between the manipulability of a master robot and the performance of a teleoperated surgical system emulating a micro-neurosurgical task.

In telerobotic surgical applications, the master robot's workspace, maneuverability, degrees of freedom, and sensory feedback should ideally match the intuitive movements of the surgeon's hand and mimic the experience and sensation of conventional surgery. The master robots currently used in surgery present several drawbacks, such as the kinematic mismatch between slave and master robot, which limits the system's ability to transfer the slave robot's dexterity and joint limits to the user. We propose a framework for the implementation of redundant master robots in surgical teleoperation tasks to overcome these issues. By employing a redundant master robot, a general redundant haptic device can be developed that is kinematically compatible with different slaves, tasks, and applications. We propose a teleoperation manipulability index (TMI) for

quantifying the dexterity of master-slave robots. Moreover, the index is used in the optimal control of a teleoperation system benefiting from a redundant master robot. The controller uses the redundancies of the robot to optimize the proposed manipulability index and kinematically match the slave and master robots. We demonstrate that by employing the proposed teleoperation manipulability and kinematic redundancies, we are able to enhance the user's control over force/velocity of the surgical robot and optimize the users' control effort while avoiding singularities and join limits of the master and slave robots.

The rest of the paper is organized as follows: In Section 2, the teleoperation manipulability is introduced as a quantifiable measure of a master-slave robotic system. In Section 3, an optimal controller is introduced that employs the kinematic redundancies of the master robot to optimize the teleoperation manipulability during a teleoperation task. Experimental and simulation results to validate the performance of the proposed controller and teleoperation manipulability measure are presented in Section 4.1 and Section 4.2, respectively. Concluding remarks appear in Section 5.

Below, first, we introduce the manipulability index for teleoperated systems, based on our previous work on the teleoperation manipulability of non-redundant robots, presented in [23]. The TMI is a measure of kinematic similarity between the master and slave robots. Next, we employ a teleoperation control strategy that uses the kinematic redundancies in the master robot to optimize the TMI. Application of this controller in enhancing the performance of a teleoperation task in terms of human-user effort and task performance are investigated in Sections 4.1 and 4.2.

2. Manipulability of Teleoperated Systems

For a robotic system, the transformation from the velocity of the end-effector in Cartesian space to the actuated joint velocities can be realized using the Jacobian matrix

$$\begin{bmatrix} \dot{x}_t \\ \dot{x}_r \end{bmatrix} = \begin{bmatrix} J_t \\ J_r \end{bmatrix} \dot{q} \tag{1}$$

where $\dot{q}$ is an n-dimensional vector that represents a set of actuated joint rates, $\dot{x}_t$ is a t-dimensional output translational velocity vector, and $\dot{x}_r$ is a r-dimensional output orientational velocity vector of the end-effector. J_t and J_r are the $t \times n$ translational and $r \times n$ orientational Jacobian matrix, respectively. It should be noted that the velocity of end-effector in Cartesian space is an m-dimensional vector where $m = t + r$, and for the case of redundant manipulator $n > m$. The Jacobian matrix is partitioned into translational and rotational parts to distinguish translational and orientational manipulabilities [25], which have different units.

A unit sphere, $\|\dot{q}\|^2 = 1$, in R^n can be mapped into an ellipsoid in R^m as shown below:

$$\begin{aligned} \|\dot{q}\|^2 = \dot{q}^T\dot{q} = \dot{x}^T(J^\dagger)^T(J)^\dagger\dot{x} = \\ \dot{x}^T(JJ^T)^\dagger\dot{x} \leq 1, \end{aligned} \tag{2}$$

where $J^\dagger$ is the pseudo-inverse of Jacobian, $J^\dagger = J^T(JJ^T)^{-1}$. In the case that the Jacobian is near the singularity, the inverse can be numerically estimated via the damped least-squares method [26]. Now, using the translational and orientational Jacobians, the translational velocity manipulability ellipsoid (TME) $\mathcal{M}_t = J_tJ_t^T \in R^t$ and orientational velocity manipulability ellipsoid (OME) $\mathcal{M}_r = J_rJ_r^T \in R^r$ are defined.

The velocity ME is a useful tool for visualizing the velocity transmission characteristics of a manipulator at a given posture. The velocity transmission shows the transformation of velocity from joint space to the Cartesian space in any direction. The directions of the principal axes of the ellipsoid are the optimal directions for effecting velocity and are determined by the eigenvectors of the matrix $\mathcal{M}_i = J_iJ_i^T$, $i = t, r$. The magnitudes of the axes are equal to the square roots of the eigenvalues of $\mathcal{M}_i$. The velocity transmission along an arbitrary direction $u_i \in R^i$, $i = t, r$, in the Cartesian space can be calculated as [27]

$$\sigma_i = \left(u_i^T(J_iJ_i^T)^\dagger u_i\right)^{-\frac{1}{2}}, \quad i = t, r. \tag{3}$$

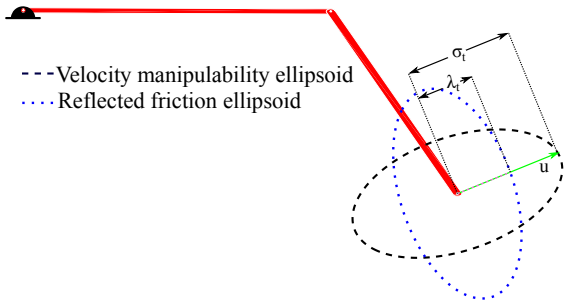

Fig. 1. The velocity transmission σ_t and reflected friction factor λ_t for a 2-DoF planar robot along direction u.

Inspired by definition of force manipulability ellipsoid [18], the reflected friction ellipsoid at the end-effector of the robot can be obtained as

$$\|F_q\|^2 = F_q^T F_q = F_x(JJ^T)F_x \leq 1, \tag{4}$$

where F_q is the $n \times 1$ vector of the joint friction torques and F_x is the $m \times 1$ vector of friction forces/torques reflected at the end-effector. Similar to the velocity transmission concept, a reflected friction factor is defined which shows the reflection of the joint friction at the end-effector of the robot. Now, by partitioning the Jacobian matrix into translational and orientational parts, the reflected friction factor along an arbitrary direction u_i, $i = t, r$, is calculated as

$$\lambda_i = \left(u_i^T(J_i J_i^T)u_i\right)^{-\frac{1}{2}}, \quad i = t, r. \tag{5}$$

By comparing (3) and (5), it can be seen that the velocity transmission σ_i is the reciprocal of the reflected friction factor λ_i along the same direction. This means that along the direction where the velocity transmission is maximized, the joints friction force reflected at the end-effector is minimized. As the result, when the user moves the end-effector of the master robot along the maximised velocity transmission direction, he/she will feel the least amount of joint friction. The velocity transmission and reflected friction factor along u for a 2-DoF planar robot in a sample configuration are shown in Fig. 1.

Now, we propose to expand the definition of ME to analyze the manipulability of teleoperated master-slave robotic systems. Considering that the master robot and the

slave robot follow each other position, we consider that the end-effector of the master robot and the end-effector of the slave robot are physically attached together. This is similar to two co-operative robots manipulating a mass-less point object with tight grasps. Therefore, co-manipulation using two robotic arms introduces new kinematic constraints on the manipulability of each arm. Here, to illustrate the concept of teleoperation manipulability, it is considered that the end-effectors of the two robots are rigidly connected. In a teleoperated system, usually, a PD controller is used for the position/force control of the master and slave robots, which does not represent a rigid connection between the end-effectors. However, for clarity and simplicity, in this paper, the above concept is introduced for an ideal transparent master-slave system. In reality, there are tracking error dynamics in the transient phase caused by the limited performance of Cartesian-space position controllers. As the tracking error in static conditions converges to zero, the Cartesian-space position controller has minimal effect on the performance of the proposed method. Also, as long as stability is preserved, high-gain robot position control in the Cartesian space can be used to diminish the distorting effect of the neglected errors on internal motion control for kinematic matching.

Following the approach presented in [23], the combined ME of two arms (slave and master robot in teleoperation context) is the largest ellipsoid that can be fitted into the intersection of the ME of the master robot and the ME of the slave robot. It should be noted that the teleoperation task is defined in the slave robot workspace, and the ME of the master robot is transformed into the task frame, i.e., the slave robot frame. By maximizing the intersection of the MEs (or minimizing the difference between the MEs), we can enhance the kinematic similarity between the slave and master robots, thus increasing the manipulability of the teleoperated system.

Motivated by the above discussion, we propose a new teleoperation manipulability index as the Jensen-Bregman Metric [28] for the distance between the MEs of the slave robot and the MEs of the master robot. The manipulability ellipsoid, $\mathcal{M}$, belongs to the set of symmetric positive definite (SPD) matrices which describe the interior of the convex

cone. The Jensen-Bregman Metric is selected as it forms a convex optimization problem that ensures convergence and also it is computationally efficient [28]. The proposed TMI is defined as

$$\nu = C_1\psi_t + C_2\psi_r \tag{6}$$

where C_1 and C_2 are the scalar scaling factors, and ψ_i, $i = t, r$ is

$$\psi_i = \texttt{logdet}(\frac{{}^s\mathcal{M}_i + {}^m\mathcal{M}_i}{2}) - \frac{1}{2}\texttt{logdet}({}^s\mathcal{M}_i{}^m\mathcal{M}_i) \tag{7}$$

where ${}^s\mathcal{M}_i$ and ${}^m\mathcal{M}_i$, the subscript $i = t$ for the translational and $i = r$ for the orientational, are the ME of slave robot and master robot, respectively. ν is an index that quantifies the kinematic similarity between the master and slave robots MEs in task space. When ν is zero the master and slave robots have similar MEs. Thus, the intersection of manipulability MEs and teleoperation manipulability are maximized.

In the next section, we will design an optimal control strategy that optimizes ν as the TMI for a redundant master robot during a teleoperation task.

3. Proposed Optimal Control of Redundant Master Robot

As discussed in Section 1, kinematic redundancy of the manipulators can offer greater flexibility to the end user to execute complicated surgical tasks. In this section, we propose an approach to improve the teleoperation manipulability introduced in Section 2 using the robot kinematic redundancy. Previously, researchers have used null-space controllers in teleoperated systems to make use of the redundant DoFs of the master linkage system with the aim of driving the master linkage away from singularities, keeping the linkage in a preferred configuration, or providing the largest possible range of motion available to the user [17]. Our proposed approach will achieve all the above goals via matching the slave and master robots' manipulability ellipsoids by minimizing the constrained teleoperation manipulability.

In teleoperated systems, the master robot and the slave robot usually have different kinematics. Therefore, they have different singularity points in their common workspace. As a result, the user can move the master robot even if the slave robot is in the singular configuration. Here, the kinematics of the redundant master robot is matched to that of the slave robot so that the singularities will occur for both robots at the same point in the workspace. This is advantageous as a unified singularity avoidance/resolution scheme will suffice for both robots. It worth mentioning that at the singular configuration of the master or slave robot, the manipulability of the redundant master robot cannot be matched with that of the slave robot. However, a singular configuration will not happen instantaneously (unless we choose the initial configuration of the robots to be where the singularity is). As the manipulability ellipsoid of the master robot is matched to that of the slave robot prior to the singular configuration, both robots will gradually approach the singular configuration together.

In our approach, it is assumed that we are implementing a general redundant master robot to teleoperatively control slave robots that are designed for a specific task. Thus, the slave robot is kinematically compatible with the desired task. We also note that the slave robot can be redundant as well, and can have its null-space controller. In this work, we have considered unilateral teleoperation in which an impedance controller and a position controller are designed for the master robot and the slave robot, respectively. Here we demonstrate that the teleoperation performance will be improved in the unilateral case, and we intend to study the bilateral case in our future work.

The proposed redundant master robot is considered as an impedance-type device. Therefore, an impedance controller needs to be designed for this device. The dynamic model of a master robot in the joint space can be defined by

$$M_q(q)\ddot{q} + C_q(q,\dot{q})\dot{q} + G_q(q) + F_q = \tau_m + J^T(q)F_h, \tag{8}$$

where $M_q(q)$ is the $n \times n$ inertia matrix, $C_q(q,\dot{q})$ is the $n \times n$ matrix of Coriolis and centrifugal terms, $G_q(q)$ is the $n \times 1$ vector of gravitational torques, τ_m is the $n \times 1$

control torque, and F_h is the $m \times 1$ torque/force applied by the user's hand on the end-effector of the master robot.

The end-effector dynamics of the master robot in the task space can be written as [29]

$$M_x\ddot{x} + C_x\dot{x} + G_x + F_x = F_m + F_h \tag{9}$$

where $M_x = (JM_q^{-1}J^T)^{-1}$ is the $m \times m$ end-effector inertia matrix or apparent inertia, $C_x = M_x(JM_q^{-1}C_q - \dot{J})J^{\#}$ is the $m \times m$ matrix of the end-effector's centrifugal and Coriolis terms, $G_x = J^{\#^T}G_q$ is the vector of gravitational forces/torques and $F_x = J^{\#^T}F_q$ the vector of friction forces/torques reflected at the end-effector, and $F_m = J^{\#^T}\tau_m$ is the task space control force/torque which corresponds to the joint space control torque. $J^{\#}$ is generalized inverse of the Jacobian matrix defined as

$$J^{\#} = M_q^{-1}J^T[JM_q^{-1}J^T]^{-1}. \tag{10}$$

The task space dynamics of the master robot can be modified to an impedance model with null stiffness by choosing F_m in (9) as follows

$$F_m = -M_x(M_x^d)^{-1}B^d\dot{x} + M_x(M_x^d)^{-1}(F_h) - F_h + C_x\dot{x}_x + G_x + F_x. \tag{11}$$

Thus, the reference impedance model of the master robot becomes

$$M_x^d\ddot{x} + B^d\dot{x} = F_h \tag{12}$$

where M_x^d and B^d are the desired apparent inertia and damping matrices which are positive definite.

Now, we modify the control law for a redundant master robot by selecting the desired robot's inertia equal to its apparent inertia, $M_x^d = M_x$. The reason for this is that: 1) We eliminate the need for calculating the precise model of the robot, M_x, and the user force, F_h, which is commonly noisy, time delayed, and inaccurate. 2) The master robots are designed back-drivable with low apparent inertia. 3) The robot loses its passivity and becomes unstable if one makes the apparent inertia lower than a certain physical

threshold [30]. Thus, by selecting $M_x^d = M_x$, the new control law becomes

$$F_m = -B^d\dot{x} + C_x\dot{x} + G_x + F_x, \tag{13}$$

with the corresponding joint torque control law

$$\tau_m = J^T F_m. \tag{14}$$

In practice, the real values for the parameters in (13) cannot be modeled exactly. Therefore, the impedance model of the master robot (12) can be rewritten as

$$M_x\ddot{x} + B^d\dot{x} + \mathcal{F} = F_h \tag{15}$$

where $\mathcal{F}$ is the force vector reflecting the effects of uncertainties in the dynamic parameters. For instance, the stiction term, which is part of F_x in (9) and hard to model, can be integrated into this term. The presence of $\mathcal{F}$ limits the achievable transparency of the system.

In the case of the redundant master robot, equation (9) describes only the end-effector dynamics and does not include the null-space dynamics of a redundant manipulator corresponding to the internal motion of the robot. The control actions used for achieving the internal motion (i.e., secondary objective) are bound to act in the null-space of the Jacobian matrix. Thus, the primary and secondary objectives are decoupled, and the primary controller precludes the effect of secondary objective control actions. To separate the null space and the task space controller we use the following control law [29]

$$\tau_d = \underbrace{\tau_m}_{\text{Impedance controller}} + \underbrace{(I - J^T(J^{\#})^T)(\tau_N - k_D\dot{q})}_{\text{Null space controller}}, \tag{16}$$

where τ_d is the $n \times 1$ desired joint torque vector, τ_m is the $n \times 1$ is torque vector calculated from (14), τ_N is the $n \times 1$ null-space torque vector corresponding to the secondary objective. τ_N is projected in the null space of the Jacobian through the matrix $I - J^T(J^{\#})^T$. It is an arbitrary joint torque vector acting in the Jacobians null-space, which does not produce any force/motion in task space and produces only joint space

internal motion of the robot. $-k_D\dot{q}$, with $k_D > 0$, is a suitable damping torque. The control law (16) ensures stability both for the primary and secondary tasks [31].

Now, we introduce τ_N, which accounts for secondary objective as

$$\tau_N = -\alpha \frac{\partial \nu(q)}{\partial q} \tag{17}$$

where α is a scalar step size and $\nu(q)$ is the secondary objective and calculated form (6). With this choice of τ_N, the robot tries to decrease the value of $\nu(q)$. Thus, the robot optimizes the kinematic similarity between the master and the slave robots, while executing a primary time-varying task.

We note that the gradient projection method is used in (16), which is a local optimization technique and deals with the instantaneous kinematics of motion. Global optimization techniques that minimize some performance index across a whole trajectory perform better than local optimization solutions. However, they are impractical for online feedback control, due to the heavy computational requirements and unexpected human motions.

Beside the manipulability, physical joint limits also have a major impact on the master robot and slave robot end-effectors' dexterity. In order to consider the effects of mechanical constraints, we integrated the joint-limit constrained Jacobian J_p [23] into the MEs of the master robot ${}^m\mathcal{M}$ and ME of the slave robot ${}^s\mathcal{M}$. The constrained Jacobian J_p is formed by penalizing the columns of Jacobian individually using

$$J_p^c = P^c J^c \tag{18}$$

where J^c is the c^{th} column of the robot Jacobian. P^c is the joint-wise penalization function given by

$$P^c = 1 - exp(\frac{-k_p(q_c - q_{c,min})(q_{c,max} - q_c)}{(q_{c,max} - q_{c,min})^2}) \tag{19}$$

At the joint-limits, P^c becomes zero and thus the corresponding column of the Jacobian. In the neutral position, ,$\frac{q_{c,max}+q_{c,min}}{2}$, P^c becomes close to one. The scaling coefficient k_p

specifies the functional shape in between these points. Using this penalty function, the individual columns of J are penalized when the cth joint value q_c approaches the limits $q_{c,min}$ or $q_{c,max}$. The modified cost function ν, developed using the modified Jacobian of the master and slave robots, tries to match the MEs of the master robot to the MEs of the slave robot and keep the master robot configuration away from the physical joint limits.

The proposed controller maximizes the teleoperation system's manipulability by minimizing the TMI ν. By minimizing the manipulability index, we are able to enhance the user's control over the force/velocity of the slave robot of the surgical system and optimize the user's control effort. Also, by using the index penalized Jacobian, we will prevent the master robot from approaching limits of the joints in addition to enhancing the teleoperation manipulability. Several simulations and experiments are performed in the following sections to verify the performance of the proposed controller.

4. Case study

For a case study, simulations and experiments are performed on a master-slave robotic system comprised of a planar four degree of freedom (DoF) master robot and two DoF planar slave robot. The 4 DoF master robot is made of two serially connected robots, a two DoF PHANToM 1.5A robot (Geomagic Inc., Morrisville, NC, USA) connected to a two DOF planar upper-limb rehabilitation robot 1.0 (Quanser Inc., Markham, ON, Canada). The base joint of the 3-DoF PHANToM robot has been removed to turn it into a 2-DoF planar robot. The slave robot is the upper-limb rehabilitation robot 2.0 (Quanser Inc., Markham, ON, Canada), which has relatively larger links and range of motion than the rehabilitation robot 1.0. The master and slave robots used in the simulations and experiments are shown in Fig. 2.

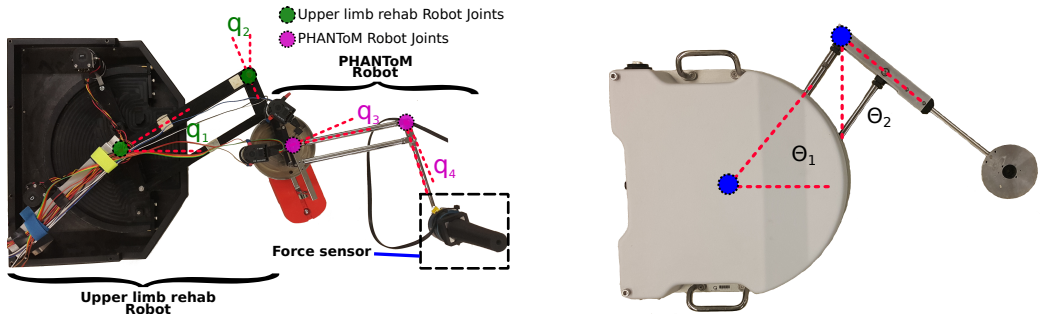

(a) (b)

Fig. 2. (a) Top view of the Master robot. (b) Top view of the Slave robot.

The Jacobians of the master and the slave robots in their base frames are

$$J_m = \begin{bmatrix} -d_1 sq_1,\ d_2 cq_2 - d_3 sq_{23} + d_4 cq_{24},\ -d_3 sq_{23},\ d_4 cq_{24} \\ d_1 cq_1,\ \ d_2 sq_2 + d_3 cq_{23} + d_4 sq_{24},\ \ d_3 cq_{23},\ \ d_4 sq_{24} \end{bmatrix} \tag{20a}$$

$$J_s = \begin{bmatrix} -l_1 s\theta_1,\ l_2 c\theta_2 \\ l_1 c\theta_1,\ \ l_2 s\theta_2 \end{bmatrix} \tag{20b}$$

where q_i $(i = 1, 2, 3, 4)$ is the master robot joints angle, θ_i $(i = 1, 2)$ is the slave robot joints angle, s and c are shorthand notations for $sin(.)$ and $cos(.)$, $q_{ij} = q_i + q_j$, and J_m and J_s are the Jacobian matrix of the master robot and slave robot, respectively. A schematic of the master robot and its DoFs is shown in Fig. 3. The links' length of the master robot and the slave robot are given in meters as $d_i = [0.254,\ 0.1405,\ 0.21,\ 0.181]$ and $l_n = [0.34,\ 0.375]$, respectively. The master robot joints' limits are defined as

$$Q_i^{min} = [-55,\ 0,\ -55,\ -20] \quad \text{degrees},$$

$$Q_i^{max} = [90,\ 145,\ 115,\ 80] \quad \text{degrees}.$$

Also, the following constraints are imposed due to structure of the robot

$$35^\circ \leq q_1 - q_2 + 90^\circ \leq 145^\circ$$

$$35^\circ \leq q_3 - q_4 + 90^\circ \leq 145^\circ.$$

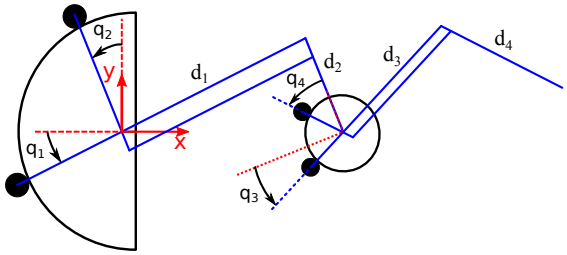

Fig. 3. Schematic of the four DoF master robot

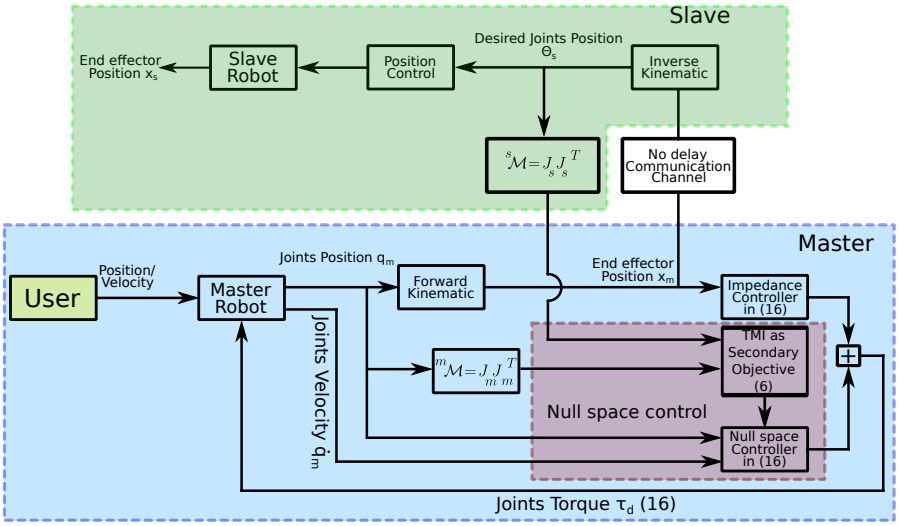

Fig. 4. Block diagram of the unilateral teleoperation system.

The dynamics of the master robot is obtained based on the works of [32] and [33]. As we are considering the unilateral teleoperation in this research and a position-based controller is used for the slave robot, the dynamics of the slave robot is neglected. A block diagram of the unilateral teleoperation system with a kinematically redundant master robot is shown in Fig. 4.

It should be noted that the robots are planar and only perform translational tasks in Cartesian space. Therefore, the manipulability ellipsoid and the cost function for the null-space controller are simplified to the translational part. Here, we considered a non-redundant two DoF robot as the slave robot. However, the slave robot can also be redundant and has its own secondary objective.

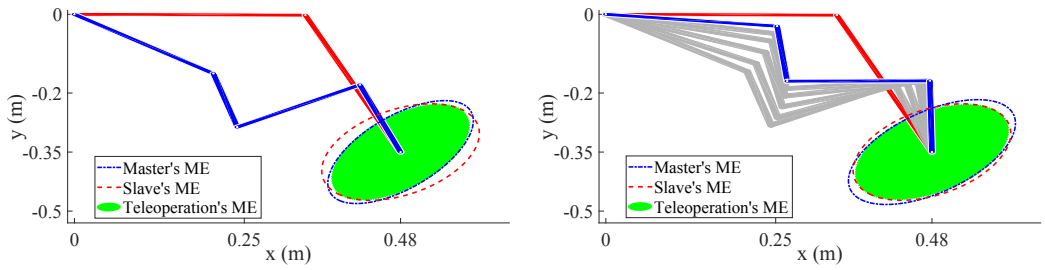

(a) (b)

Fig. 5. Comparison between the manipulability ellipsoids of the slave, master, and teleoperated system. (a) Initial configuration of the master robot. (b) Evolution of the master robot configuration and the final configuration with manipulability optimization. The master and slave robots are shown in solid blue and red, respectively. The evolution of the master robot configuration in time is shown in grey.

4.1. Simulation Studies

In the first simulation study, the end-effector of the master and slave robot are fixed at a certain point in the XY plane. Then, the null-space controller is used to minimize ν (i.e., maximize the teleoperation manipulability). The results of simulations are shown in Fig. 5. The configuration of the master and slave robots, the corresponding velocity MEs, and the intersection of the slave and master robot MEs (i.e., the teleoperation manipulability ellipsoid) with and without the null space controller are shown.

In the simulation, the master and slave robots' end-effector position are initially at $(X, Y) = [0.48m,\ -0.35m]$. The initial configuration of the master robot is selected as

$$q_i = [-0.63,\ 0.25,\ 0.28,\ 0.09]^T rad.$$

The values of desired damping parameter is $B^d = \text{diag}\{0.3,\ 0.3\}$Ns/m. B^d is chosen sufficiently small such that the free space force ($F_h \to 0$) and the stability are achieved. Also, the uncertainty term in (15) is modeled as

$$\mathcal{F} = J^{\#^T} F_q^{un} = J^{\#^T} \Gamma \dot{q} \tag{21}$$

where F_q^{un} is the uncertainty term in the joint space and Γ is approximated equal to $\text{diag}\{0.01,\ 0.01,\ 0.01,\ 0.01\}$.

As shown in Fig. 5, by using the null space controller, the configuration of the master robot changes to maximize the teleoperation ME, while the end-effector of the master and slave robots are fixed. The area of the teleoperation ME is increased by 18.1% via the null space controller.

In the next simulation study, it is considered that the slave robot follows the master robot's end-effector position, and the master robot follows a given trajectory in the slave's workspace. Control input defined in (16) is used to maximize the teleoperation manipulability while following the given trajectory in the slave robot's workspace with a constant speed of $2cm/s$. To achieve this, an internal PD controller is designed to change the external force, F_h, such that the end-effector of the robot follows the trajectory with the given constant speed.

To show the advantages of the proposed control strategy, the results are compared to unilateral teleoperation control with 1) a two DoF master robot which is made by fixing the last two DoFs of the redundant master robot, i.e., θ_3 and θ_4 in Fig. 3 are fixed at zero degree and will be called Rehab robot hereafter, and 2) a null space controller that only optimizes the kinematics manipulability of the master robot. The second controller can be achieved by selecting the null space controller input as $\tau_N = \alpha \dfrac{\partial \mu(q)}{\partial q}$, where μ is the classic manipulability index of a single robot defined as [18]

$$\mu(q) = \sqrt{\det(J_m J_m^T)} \tag{22}$$

A "W-shaped" curve that follows various points in the slave robot's task space is selected as the robot's trajectory (see Fig. 6). The reference trajectory is selected to, 1) cover most of the slave robot's workspace, 2) be in the two DoF master robot's workspace, and 3) be aligned with the major axis of the slave robot's ME. As shown in Fig. 6, although the redundant master robot and the two DoF master robot have links of the same length, the redundant master robot has a bigger workspace compared to the two DoF master robot. This is one of the advantages of the redundant master robot over the traditional non-redundant master robots.

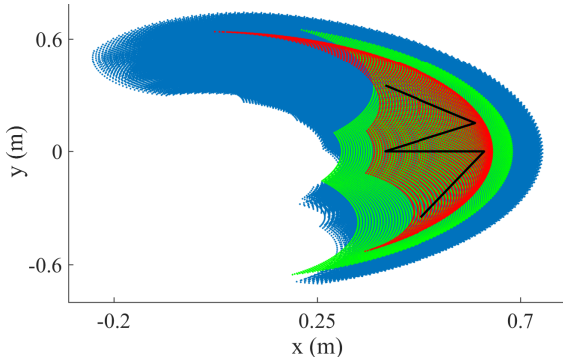

Fig. 6. Redundant master robot's workspace (blue dots), two DoF master robot's workspace (red dots), slave robot's workspace (green dots), and reference trajectory (solid black line) are shown.

Fig. 7 shows a comparison of simulation results for three scenarios: 1) The redundant master robot with the proposed teleoperation manipulability optimizer. 2) The redundant master robot with its manipulability optimizer. 3) The Rehab robot. It can be seen that the ME of the master robot is maximized in the case of the redundant master robot with its manipulability optimizer (see Fig. 7(b)). However, the teleoperation ME is smaller than the teleoperation ME as the kinematics of the slave robot is not considered. The mean area of the teleoperation manipulability is 0.1034 when the master robot's manipulability is optimized, which is 15.3% less than the mean area of the teleoperation manipulability when our proposed approach is employed.

Fig. 7(a) shows a comparison between the master robot ME, the slave robot ME, and the teleoperation ME over the given trajectory for the case of a redundant robot with the proposed teleoperation manipulability optimizer. It can be seen that the proposed redundancy resolution is effective, and the ME of the master robot matches the ME of the slave robot, and the teleoperation manipulability is improved. The ME of the Rehab robot is compared with the ME of the rehabilitation robot 2.0 in Fig. 7(c). This figure shows the difference in the kinematics of the Rehab robot and the slave robot.

Another way to show the effectiveness of the proposed approach is to compare the user effort in the three control scenarios. Considering the conservation of energy, the

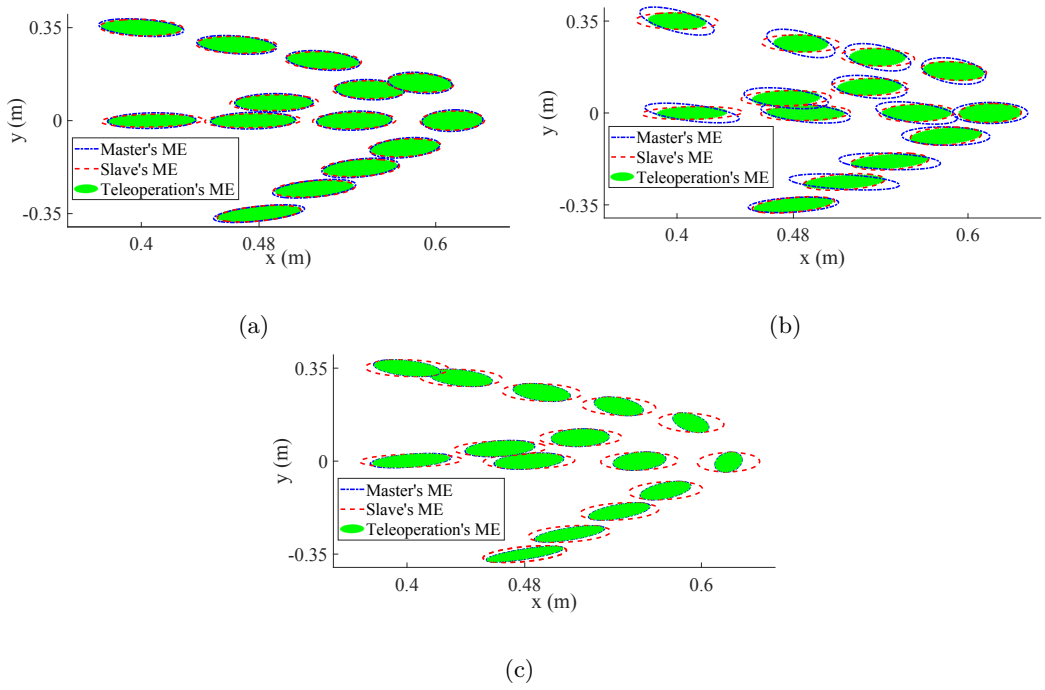

Fig. 7. Simulation results for trajectory tracking (a) with redundant master robot with the teleoperation manipulability optimization, (b) with redundant master robot with the master robot's manipulability optimization, and (c) with non-redundant two DoF master robot. The manipulability ellipsoids of the slave, master, and teleoperated system during trajectory tracking are shown.

work done by the user is measured as

$$W = \int_0^T F_h^T \dot{x} dt, \tag{23}$$

where $\dot{x}$ is the velocity of the master robot end-effector, which is equal to the velocity of the user's hand, and F_h is the forces applied by the user.

Now we use (23) to estimate the human user effort over time during the trajectory tracking scenario. The same value for the B^d is chosen for all simulation studies. Results are shown in Fig. 8. As it can be seen in this figure, the energy used to move the slave robot to follow the W-shaped trajectory for our proposed null-space controller is less than the two other approaches. This difference grows with time, which will have a significant impact on the performance of the user in a relatively long teleoperation task. This is important especially in the long surgeries in which the surgeon makes better decisions when he/she is less tired [34].

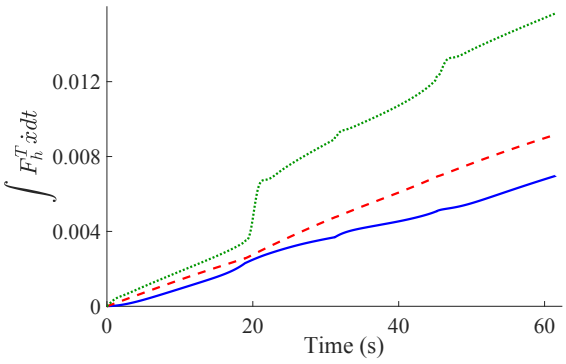

Fig. 8. A comparison between the user's effort for controlling the position of the slave robot with the proposed teleoperation manipulability optimization for redundant master robot (Solid blue line), master robot manipulability optimization for redundant master robot (Dashed red line), and two DoF non-redundant master robot (Doted green line).

4.2. Experiments

In this section, experiments are performed to evaluate the performance of the proposed controller. The setup is shown in Fig. 2 is used to perform the experiments. For interfacing the robots with the computer, MATLAB/Simulink (MathWorks Inc., Natick, MA, USA) with Quarc real-time control software (Quanser Inc., Markham, ON, Canada) is used. In the experiments, eight users (6 males and 2 females), all right-handed, were asked to move the master robot so that the slave robot end-effector would follow the same reference trajectory from the simulation studies. Also, they were asked to take the path following accuracy as the primary objective and the task's completion time as the secondary objective. The reference trajectory and the position of the slave robot end-effector were shown to the user in real-time. Before starting the experiments, the subjects were asked to perform a training run to become familiar with the experimental setup. The users had some exposure to the haptic devices and teleoperation systems.

Three different scenarios were implemented in the experiments: 1) unilateral teleoperation with the redundant master robot and proposed teleoperation manipulability as the null-space controller, 2) unilateral teleoperation with the redundant master robot and the manipulability of the master robot as the null-space controller, and 3) unilateral teleoperation with non-redundant two DoF master robot. In this paper, in

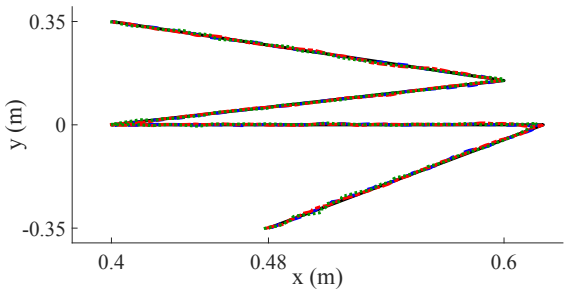

Fig. 9. Reference (Solid black line), Scenario 1 (Blue Dashed line), Scenario 2 (Red Dashed-dot line), and Scenario 3 (green dot line) paths of user #3 for trajectory following task.

order to isolate the positive impact of the master robot's redundancy on users during trials, the experiments are performed with a unilateral teleoperated system. In a bilateral teleoperation experiment, the absence of full transparency would have made it difficult to isolate the impact of the redundancy of the master robot because there are so many other factors at play.

In the above scenarios, the same position controller (i.e., a PD controller) is used for the slave robot. The following Cartesian-space control law used for the master robot in the experiments:

$$F_m = -B^d \dot{x} + C_x \dot{x} \tag{24}$$

In each trial, one of the master robots were presented to the user. Thus each user performed three trials. The trials were presented in a randomized order to the users to minimize the effect of learning in the study. The same desired damping parameter, B^d, as the simulation studies is used in the experiments (i.e., $B^d = \text{diag}\{0.3,\ 0.3\}\text{Ns/m}$). Also, the friction forces, F_x, is not compensated for the experiments.

To compare the performance of the user in the three scenarios, the trajectory tracking error, the user's effort, and the execution time of the trajectory are considered as the performance metrics. The sample representative results of the end-effector movement for the three experimental scenarios of the user #3 as well as the reference trajectory are shown in Fig. 9.

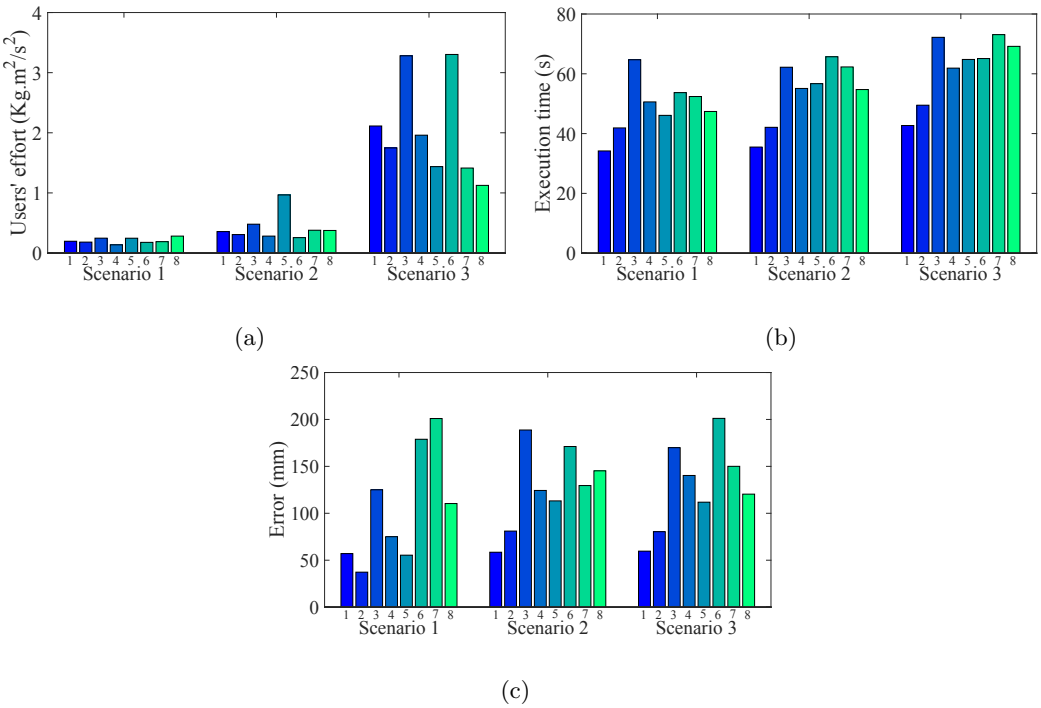

Fig. 10. Bar plot results for (a) Users' effort, (b) Execution time, and (c) Trajectory tracking error.

The trajectory tracking error is defined as the norm of the distance between the desired trajectory and the user's actual trajectory ($error = \|L_d - L_t\|$). In order to compare the user's effort during the trajectory following task, (23) is used to measure the work done by the user. The forces are measured via a 6 DoF force/torque sensor (50M31A3-I25, JR3 Inc., Woodland, CA, USA) placed on the master robot's user interface (see Fig. 2).

The experiment results are summarized in Table I. The mean values for the trajectory error, the execution time, and the user's effort are smaller in scenario one than in the other two scenarios. This demonstrates the enhanced control of the user over the slave robot's trajectory and improved accuracy of the proposed null space controller compared to previously used methods.

The test results for the three performance metrics are shown as bar graphs in Fig 10. Fig 10(a) shows the results of all trials for the users' effort in the three scenarios. A one-way ANOVA test was used to investigate further, which confirms a significant difference between the scenarios ($F(2, 21) = 32.63$, $p = 3.61E - 7$). Also, the paired-sample t-test indicates that the users' effort in each scenario was statistically different from every other

Table I . Mean and Std Values for the Performance Metrics in each Scenarios .

	Scenario 1	Scenario 2	Scenario 3
User's effort ($Kg.m^2/s^2$)	0.207 (std=0.047)	0.425 (std=0.229)	2.048 (std=0.830)
Task completion time (s)	48.8 (std=8.9)	54.3 (std=10.4)	62.3 (std=10.8)
Trajectory error (mm)	105.0 (std=60.2)	126.5 (std=43.3)	129.2 (std=46.3)

Table II . Hypotheses and adjusted p-values of t-test for the excecution time .

Hypothesis	p-value	Significant
Scenario 1 < Scenario 2	0.0245	True
Scenario 1 < Scenario 3	0.00039	True
Scenario 2 < Scenario 3	0.0012	True

scenario ($p \leq 0.05$). The P-values are adjusted with the False Discovery Rate (FDR) method.

Fig. 10(b) shows the experimental results for the execution time for the three different scenarios. As stated in Table I, the users completed the task with the lowest time in scenario one. The statistical significance of the results is confirmed by using the one-way ANOVA test ($F(2, 21) = 3.57$, $p = 0.046$). In order to further investigate this, a paired-sample t-test was used between different pairs of scenarios. The results of the t-test are shown in Table II.

Fig. 10(c) shows the trajectory following error for all users in three scenarios. This graph does not show any clear trend for the trajectory following error. Also, a one-way ANOVA test for the three scenarios ($F(2, 21) = 0.55$, $p = 0.583$) shows that there is no statistically significant difference between the trajectory following errors. This is as the result of the fact that the users have been told to perform the path taking into account

the accuracy as a primary objective. Thus, the error is similar for the three scenarios, but the task completion time and users' effort is significantly smaller for scenario one.

It should be noted that changing the damping parameter B^d in software has a considerable impact on the user's effort in a given task [35]. For this reason, in our experiments, the same damping was used for the three different master robots (Scenario 1, Scenario 2, and Scenario 3). The difference between the users' efforts in each scenario was because of the difference in the robots' kinematics (redundancy vs. non-redundancy) and configuration (due to different cost functions for the redundant case), which affected the friction reflected to the users' hand. The overall finding was that when the kinematics of the redundant master robot matches to that of the slave robot, the user had to apply the least effort to perform the task.

As stated before, it is considered that the slave robot is properly designed for the given task (e.g., a particular trajectory-following task). This assumption means that the major axis of the manipulability ellipsoid of the slave robot is aligned with the desired trajectory direction. The optimal direction for affecting velocity as well as the optimal direction to control the force is along the major axis of the manipulability ellipsoid (ME). This means that for a robot, along the major axis of the ME, the user can move the end-effector with minimum movements of the robot's joints (i.e., feeling the least amount of joint frictions). By matching the ME of the master robot to that of the slave robot, the major axis of the ME of the master robot will be aligned to the desired task as well. This consequently minimizes the reflected joints friction at the end-effector of the master robot, which was not compensated for in the experiments.

The proposed approach can be used in practice to minimize the effects of friction, which is of practical importance as the robot joint friction is hard to model and identify. For instance, once a desired task-dependent damping for the master robot is determined and programmed in software, we can ensure that the effects of robot joint friction are minimal such that the total damping that the user experiences is close to the desired robot damping.

5. Concluding Remarks and Future Work

In this paper, we proposed a quantifiable measure of manipulability of master-slave robotic systems. The application of the proposed measure in designing an optimal controller, which can enhance the manipulability of the system, was demonstrated. We evaluated the enhanced performance of the proposed approach via a comparison with two other existing control strategies. It was shown that by implementing our controller in a robotic master-slave system that benefits from a redundant master robot, we are able to improve the overall manipulability of the system, which can improve the user's control over slave robot's end-effector force/velocities and reduce the user's control effort. In future, the proposed manipulability optimization method will be used on more complex teleoperation system with more DoFs. Here, we used a unilateral teleoperated systems to investigate the proposed method with near-ideal transparency and without any communication delay. In the future, a bilateral teleoperated master-slave system will be considered. We will also use the manipulability criterion in motion planning of surgical tasks for complex surgical procedures.

Acknowledgements

This research was supported by the Canada Foundation for Innovation (CFI) under grants LOF 28241 and JELF 35916, the Alberta Innovation and Advanced Education Ministry under Small Equipment Grant RCP-12-021, the Alberta Economic Development and Trade Ministry under Small Equipment Grant RCP-17-019, the Natural Science and Engineering Research Council (NSERC) of Canada under the Collaborative Health Research Projects (CHRP) Grant 316170, the Government of Alberta's grant to Centre for Autonomous Systems in Strengthening Future Communities, and the Quanser, Inc.

References

1. P. Berkelman and J. Ma, "A compact modular teleoperated robotic system for laparoscopic surgery," *The International Journal of Robotics Research*, vol. 28, no. 9, pp. 1198–1215, 2009.

2. H. Kolbari, S. Sadeghnejad, M. Bahrami, and K. E. Ali, "Adaptive Control of a Robot-Assisted Tele-Surgery in Interaction With Hybrid Tissues," *Journal of Dynamic Systems, Measurement, and Control*, vol. 140, no. 12, 08 2018.
3. V. Hayward and O. R. Astley, "Performance measures for haptic interfaces," in *Robotics Research*, G. Giralt and G. Hirzinger, Eds. London: Springer London, 1996, pp. 195–206.
4. A. R. Licona, F. Liu, D. Pinzon, A. Torabi, P. Boulanger, A. Lelevé, R. Moreau, M. T. Pham, and M. Tavakoli, *Applications of Haptics in Medicine*. Cham: Springer International Publishing, 2020, pp. 183–214.
5. R. Ellis, O. Ismaeil, and M. Lipsett, "Design and evaluation of a high-performance haptic interface," *Robotica*, vol. 14, no. 03, p. 321, 1996.
6. B. Siciliano, "Kinematic control of redundant robot manipulators: A tutorial," *Journal of Intelligent and Robotic Systems*, vol. 3, no. 3, pp. 201–212, 1990.
7. Y.-C. Liu and N. Chopra, "Controlled synchronization of heterogeneous robotic manipulators in the task space," *IEEE Transactions on Robotics*, vol. 28, no. 1, pp. 268–275, Feb 2012.
8. D.-Y. Hwang and B. Hannaford, "Teleoperation performance with a kinematically redundant slave robot," *The International Journal of Robotics Research*, vol. 17, no. 6, pp. 579–597, 1998.
9. N. Nath, E. Tatlicioglu, and D. M. Dawson, "Teleoperation with kinematically redundant robot manipulators with sub-task objectives," *Robotica*, vol. 27, pp. 1027–1038, 2009.
10. H. Das, T. B. Sheridan, and J. J. E. Slotine, "Kinematic control and visual display of redundant teleoperators," in *Conference Proceedings., IEEE International Conference on Systems, Man and Cybernetics*, Nov 1989, pp. 1072–1077 vol.3.
11. Y.-C. Liu, "Task-space bilateral teleoperation systems for heterogeneous robots with time-varying delays," *Robotica*, vol. 33, no. 10, p. 2065–2082, 2015.
12. F. Ficuciello, L. Villani, and B. Siciliano, "Variable impedance control of redundant manipulators for intuitive human – robot physical interaction," *Transactions on Robotics*, vol. 31, no. 4, pp. 1–14, 2015.
13. M. Mihelj, "Human arm kinematics for robot based rehabilitation," *Robotica*, vol. 24, no. 3, p. 377–383, 2006.
14. S. Schaal and N. Schweighofer, "Computational motor control in humans and robots," *Current Opinion in Neurobiology*, vol. 15, no. 6, pp. 675 – 682, 2005, motor sytems / Neurobiology of behaviour.
15. I. Nisky, M. H. Hsieh, and A. M. Okamura, "Uncontrolled manifold analysis of arm joint angle variability during robotic teleoperation and freehand movement of surgeons and novices," *IEEE Transactions on Biomedical Engineering*, vol. 61, no. 12, pp. 2869–2881, dec 2014.
16. M. Ueberle, N. Mock, and M. Buss, "VISHARD10, a novel hyper-redundant haptic interface," in *Proceedings - 12th International Symposium on Haptic Interfaces for Virtual Environment and*

Teleoperator Systems, HAPTICS, 2004, pp. 58–65.

17. J. K. Salisbury Jr, A. J. Madhani, G. S. Guthart, G. D. Niemeyer, and E. F. Duval, "Master having redundant degrees of freedom," 2004, US Patent 6,684,129.
18. T. Yoshikawa, "Manipulability of Robotic Mechanisms," *The International Journal of Robotics Research*, vol. 4, no. 2, pp. 3–9, 1985.
19. O. Flores-Díaz, I. Juárez-Campos, and J. Carrera-Bolaños, "Procedures to determine the principal directions of kinematic performance in serial robots," *Robotica*, vol. 36, pp. 1664–1679, 2018.
20. J. Angeles and F. C. Park, *Performance Evaluation and Design Criteria*. Springer Berlin Heidelberg, 2008, pp. 229–244.
21. R. Konietschke, T. Ortmaier, H. Weiss, G. Hirzinger, and R. Engelke, *Manipulability and Accuracy Measures for a Medical Robot in Minimally Invasive Surgery*. Springer Netherlands, 2004, pp. 191–198.
22. Z. Li, D. Milutinović, and J. Rosen, "Design of a multi-arm surgical robotic system for dexterous manipulation," *ASME Journal of Mechanisms and Robotics*, vol. 8, no. 6, pp. 061 017–061 027, 2016.
23. A. Torabi, M. Khadem, K. Zareinia, G. R. Sutherland, and M. Tavakoli, "Manipulability of teleoperated surgical robots with application in design of master/slave manipulators," in *2018 International Symposium on Medical Robotics (ISMR)*, March 2018, pp. 1–6.
24. Y. Maddahi, M. Greene, L. S. Gan, T. Hirmer, R. L'Orsa, S. Lama, G. R. Sutherland, and K. Zareinia, "Performance evaluation of a surgical telerobotic system using kinematic indices of the master hand-controller," in *International Conference on Human Haptic Sensing and Touch Enabled Computer Applications, EuroHaptics 2014*, M. Auvray and C. Duriez, Eds. Springer Berlin Heidelberg, 2014, pp. 167–175.
25. T. Yoshikawa, "Translational and rotational manipulability of robotic manipulators," in *Industrial Electronics, Control and Instrumentation, 1991. Proceedings. IECON '91., 1991 International Conference on*, Oct 1991, pp. 1170–1175 vol.2.
26. C. W. Wampler, "Manipulator inverse kinematic solutions based on vector formulations and damped least-squares methods," *IEEE Transactions on Systems, Man, and Cybernetics*, vol. 16, no. 1, pp. 93–101, Jan 1986.
27. B. Siciliano, L. Sciavicco, L. Villani, and G. Oriolo, *Robotics - Modelling, Planning and Control*. Springer-Verlag London, 2009.
28. A. Cherian, S. Sra, A. Banerjee, and N. Papanikolopoulos, "Efficient similarity search for covariance matrices via the jensen-bregman logdet divergence," in *2011 International Conference on Computer Vision*, Nov 2011, pp. 2399–2406.

29. O. Khatib, "A unified approach for motion and force control of robot manipulators: The operational space formulation," *IEEE Journal on Robotics and Automation*, vol. 3, no. 1, pp. 43–53, February 1987.

30. J. E. Colgate and N. Hogan, "Robust control of dynamically interacting systems," *International Journal of Control*, vol. 48, no. 1, pp. 65–88, 1988.

31. J. Nakanishi, R. Cory, M. Mistry, J. Peters, and S. Schaal, "Operational space control: A theoretical and empirical comparison," *International Journal of Robotics Research*, vol. 27, no. 6, pp. 737–757, 2008.

32. M. C. Çavuşoğlu, D. Feygin, and F. Tendick, "A critical study of the mechanical and electrical properties of the phantom haptic interface and improvements for highperformance control," *Presence*, vol. 11, no. 6, pp. 555–568, Dec 2002.

33. M. D. Dyck, "Measuring the Dynamic Impedance of the Human Arm," M.Sc. Thesis, University of Alberta, 2013.

34. R. Randell, N. Alvarado, S. Honey, J. Greenhalgh, P. Gardner, A. Gill, D. C. Jayne, A. Kotze, A. Pearman, and D. Dowding, "Impact of robotic surgery on decision making: Perspectives of surgical teams," *AMIA ... Annual Symposium proceedings. AMIA Symposium*, vol. 2015, pp. 1057–66, 2015.

35. C. Richard and M. Cutkosky, "The effects of real and computer generated friction on human performance in a targeting task," in *Proceedings of the ASME Dynamic Systems and Control Division*, vol. 69, no. 2, 2000, pp. 1101–1108.